https://doi.org/10.5194/egusphere-2025-5474
Preprint. Discussion started: 18 November 2025

OSLThermo and ESRThermo: Libraries of codes for trapped-charge thermochronometry

Chloé Bouscary[1,2,3] & Georgina E. King[1], Melanie Kranz-Bartz[1,4], Maxime Bernard[1], Rabiul H. Biswas[1,5], Lily Bossin[1,6], Arnaud Duverger[1,7], Benny Guralnik[1,8], Frédéric Herman[1], Ugo Nanni[1,9], Nadja Stalder[1], Pierre G. Valla[1,10], Vjeran Visnjevic[1,11], and Xiaoxia Wen[1]

[1] Institute of Earth Surface Dynamics, University of Lausanne, Lausanne, 1015, Switzerland
[2] Department S3 – Geochronology, LIAG-Institute for Applied Geophysics, Hannover, 30655, Germany
[3] Earth Surface Process Modelling, Helmholtz Centre for Geosciences, Potsdam, 14473, Germany
[4] Institute of Geosciences, Ruhr-University Bochum, Bochum, 44801, Germany
[5] Department of Earth Sciences, Indian Institute of Technology Kanpur, Kanpur, Uttar Pradesh, 208016, India
[6] Paul Scherrer Institute, Villigen, 5232, Switzerland
[7] Muséum National d'Histoire Naturelle, Sorbonne Université, UMR CNRS 7590, Institut de Minéralogie, de Physique des Minéraux et de Cosmochimie, Paris, 75005, France
[8] KLA Corporation, Diplomvej 373, Kgs Lyngby DK-2800, Denmark
[9] Department of Geosciences, University of Oslo, Oslo, 0371, Norway
[10] Université Grenoble Alpes, Université Savoie Mont-Blanc, CNRS, IRD, Université Gustave Eiffel, ISTerre, Grenoble, 38000, France
[11] Climate and Environmental Physics, University of Bern, Bern, 3012, Switzerland

Correspondence to: Chloé Bouscary (chloebouscary@gmail.com) & Georgina E. King (georgina.king@unil.ch)

Abstract. Over the past fifteen years, trapped-charge (T-C) thermochronometry has been established as an ultra-low temperature (<80 °C) thermochronometric system. Its novelty is its ability to resolve rock cooling within the final few km of Earth's surface, as well as rock-surface temperature changes since the Last Glacial Maximum to the present day. Deriving temperature histories from the luminescence signals of feldspar minerals, or the electron spin resonance signals of quartz minerals, requires the modelling of both signal accumulation and signal loss in response to mineral exposure to ionizing radiation and temperature, as well as athermal signal losses for feldspar minerals. Two open-source libraries have been developed in MATLAB that allow different numerical models to be used for this purpose; the first is applicable to the infra-red stimulated luminescence (IRSL) of feldspar minerals (OSLThermo) and the second to the electron spin resonance (ESR) signal of quartz minerals (ESRThermo). These libraries have been made available in GITHUB and this contribution describes their broad structure, the T-C models that have been implemented and their practical use.

Codes are available for download on GitHub: *https://github.com/GeorginaKing/OSLThermo* for luminescence thermochronometry & *https://github.com/GeorginaKing/ESRThermo* for ESR thermochronometry.

https://doi.org/10.5194/egusphere-2025-5474
Preprint. Discussion started: 18 November 2025

1 Introduction

The development of trapped-charge thermochronometry over the past fifteen years (e.g., Herman et al., 2010; Guralnik et al., 2015a; Wu et al., 2015; King et al., 2016a; Brown et al., 2017; Biswas et al., 2018; King et al., 2020; Zhang et al., 2025) and recent investigations of trapped-charge thermometry (e.g., Guralnik and Sohbati, 2019; Biswas et al., 2020) have built upon both previous applications of the method (e.g., Houtermans et al., 1957; Ronca and Zeller, 1965; Grün et al., 1999) and earlier fundamental research describing the accumulation and loss of trapped-charge signals (e.g., Prokein and Wagner, 1994; Toyoda and Ikeya, 1991). The premise of the technique is that, as the luminescence and electron spin resonance (ESR) signals of feldspar and quartz minerals are thermally sensitive, they can be used to determine temperature histories. Temperature changes occur, for example, as rocks are exhumed towards the Earth's surface (e.g., King et al., 2016c; Bouscary et al., 2024), or as atmospheric temperature changes due to climatic variations and affects rock surface temperatures (e.g., Guralnik and Sohbati, 2019; Biswas et al., 2020).

Luminescence and ESR thermochronometry have been applied in a variety of settings to determine rock-thermal histories, including the Southern Alps of New Zealand (Herman et al., 2010), the Himalayas (De Sarkar et al., 2013; King et al., 2016c; Bouscary et al., 2024), the European Alps (Lambert, 2018; Wen et al., 2024), Taiwan (Wu et al., 2015), the Chilean Andes (Stalder et al., 2022), and in the Japanese Alps (King et al., 2023; Bartz et al., 2024) and alpine foreland (Ogata et al., 2022). Recent reviews are given by King et al. (2016b) and Herman and King (2018).

Luminescence and ESR thermochronometry rely on the combination of laboratory measurements with numerical models, that allows the conversion of trapped-charge concentrations into thermal histories. Two or three laboratory experiments are typically used to build an ESR or luminescence thermochronometry measurement, respectively (e.g., Herman et al., 2010; Guralnik et al., 2015b; King et al., 2016a; Biswas et al., 2018; Fang and Grün, 2020; King et al., 2020) (Fig. 1). The first experiment (Fig. 1B and Fig. 1E) measures the concentration of trapped charge within the sample, and is usually done using a single aliquot regenerative dose method (e.g., Murray and Wintle, 2000; Tsukamoto et al., 2015). The measurement comprises construction of a sample-specific calibration curve, for sample signal response to laboratory irradiation, known as a dose response curve (DRC). As trapped-charge thermochronometry data are often described as saturation ratios, i.e. the proportion of electrons trapped (n) relative to the maximum possible number of trapped electrons (N), laboratory DRC are generally measured until signal saturation (i.e. no further increase in sample signal for increasing dose). For some samples, the exceptionally high saturation level of the quartz ESR Al-centre makes this impractical, and for this signal, the system may be treated as non-saturating (e.g., King et al., 2020). The second experiment (Fig. 1C and Fig. 1F) measures the thermal decay of the luminescence or ESR signals in response to temperature. Generally, it comprises an isothermal decay experiment whereby signal loss relative to a fixed temperature is measured following different isothermal heating durations (e.g., Bouscary and King, 2022). The final experiment is only applicable to the luminescence of feldspar minerals and consists of measuring the rate of anomalous fading (Wintle, 1973; Visocekas et al., 1994) by measuring signal loss at ambient temperature following different delay durations (Fig. 1A).

https://doi.org/10.5194/egusphere-2025-5474
Preprint. Discussion started: 18 November 2025

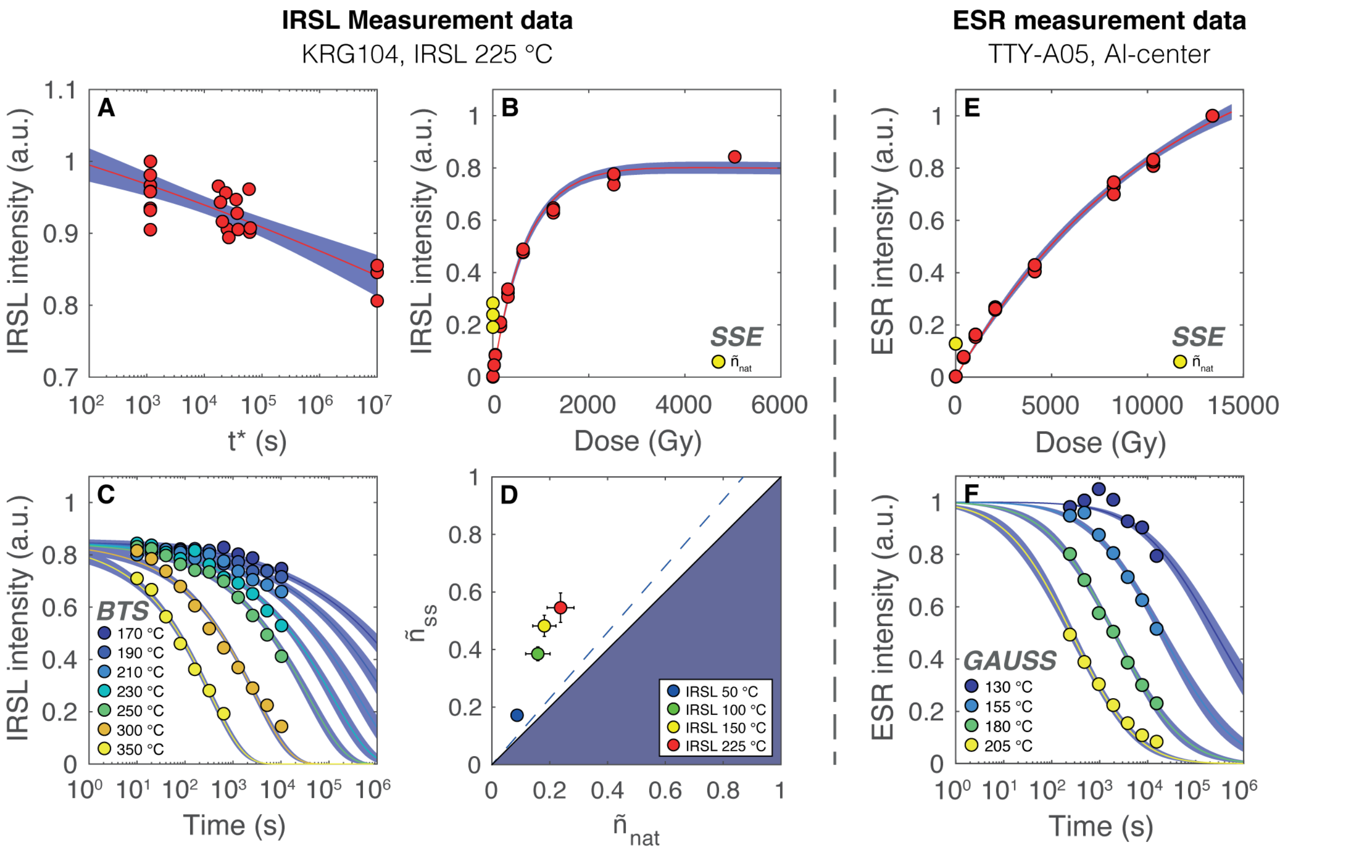

Figure 1: Experimental IRSL and ESR data together with model fits (see Section 2) for two samples from the Japanese Alps. (A) Athermal signal loss, (B) dose response, (C) and isothermal decay for the IRSL$_{225}$ signal of the K-feldspar extract of sample KRG104 (King et al., 2020). (D) Comparison of luminescence natural saturation ratios, $\tilde{n}_{nat}$, with those calculated for athermal steady state, $\tilde{n}_{ss}$, (dashed line indicates 15% deviation from unity) for the four IRSL signals of sample KRG104. (E) Dose response and (F) isothermal decay for the Al-centre of sample TTY-A05 (Bartz et al., 2024).

Fitting these experimental data using models that describe signal accumulation, thermal or athermal decay, allows the experimental data to be reduced to several kinetic parameters, as illustrated in Eq. (1):

$$\frac{\mathrm{d}\tilde{n}}{\mathrm{d}t} = \frac{\dot{D}}{D_0}\,(1-\tilde{n})^{\alpha} - s\,\tilde{n}^{\beta}\,e^{\left(\frac{-E_a}{k_B\,T}\right)} - \tilde{s}\,\tilde{n}\,e^{\left(-\rho'^{-\frac{1}{3}}r'\right)} \quad (1)$$

The trapped-charge population $\tilde{n}$ at a given time t (Ma) is given by three terms. The first term on the right-hand side of the equation describes trapped-charge accumulation where $\dot{D}$ (Gy·Ma^{-1}) is the environmental dose rate, D_0 (Gy) is the characteristic dose of saturation and α is an exponent ≥1, depending on whether electron trapping is described as first (α = 1) or general ($\alpha > 1$) order. The second term describes thermal loss at a given temperature, T (K), where s (s^{-1}) is the frequency factor, E_a (eV) is the activation energy of the electron trap, k_B (eV·K^{-1}) is the Boltzmann constant, and β the order of kinetics

https://doi.org/10.5194/egusphere-2025-5474
Preprint. Discussion started: 18 November 2025

≥1. The final term describes athermal loss where $\tilde{s}$ (3 x 10^{-15} s^{-1}) is a frequency factor, ρ' is a dimensionless description of the density of recombination centres and r' is a dimensionless distance between traps and recombination centres (Huntley, 2006). A variety of different models describing signal accumulation and athermal or thermal signal loss have been investigated for use in trapped-charge thermochronometry/thermometry applications (e.g., Guralnik et al., 2015b; Biswas et al., 2018; Lambert, 2018; Biswas et al., 2020; King et al., 2020), and have been validated against data collected in the laboratory as well as independent temperature measurements (e.g., Lambert, 2018; Bouscary and King, 2022). These kinetic parameters can then be used together with Eq. (1), to predict a trapped-charge concentration for a particular time-temperature history, allowing the natural trapped charge concentration of a sample to be inverted for its thermal history.

In this contribution, we present two MATLAB libraries, OSLThermo and ESRThermo, that are available for the processing of trapped-charge thermochronometry data. We first outline the T-C models implemented in the codes and then describe the structure of the OSLThermo and ESRThermo libraries as well as the required input format of experimental data. Note that we do not comment on the suitability of different models for specific datasets, but rather list those models that have been implemented in the libraries at present. We anticipate that these libraries will be further updated in the future.

2 Model overview

In this section, the specific T-C models implemented in the OSLThermo and ESRThermo libraries are described. Although athermal signal losses are often not measured first, here we begin with fitting these data as athermal losses must also be accounted for when constraining the trapped-charge concentration and fitting isothermal decay data of feldspar minerals in the OSLThermo library.

2.1 Athermal signal loss (OSLThermo library only)

Athermal signal losses are known to affect the luminescence of feldspar minerals (Visocekas et al., 1994) and must be accounted for when fitting luminescence data to derive the kinetic parameters of signal dose response and thermal decay. The OSLThermo library uses the model of Huntley (2006), as implemented by Kars et al. (2008), to compute the natural dose response curve of feldspar signals by correcting the data for athermal fading, and to calculate the natural steady-state luminescence signal, $\tilde{n}_{ss}$. This signal is expressed as the ratio between the trapped-charge concentration, n, and the maximum possible trapped-charge concentration in the absence of anomalous fading, N. Signal saturation is the main limitation of luminescence thermochronometry (e.g., Valla et al., 2016), and accurate screening of luminescence signals for saturation is essential.

The rate of anomalous fading induced signal loss can be calculated from:

$$n(t^*) = n(0) \cdot \varphi(t^*) \quad (2)$$

where $n(0)$ is the initial trapped-charge concentration at time 0, $n(t^*)$ is the signal remaining after fading time t^* (s), which is calculated following Appendix F of Aitken (1985), and

https://doi.org/10.5194/egusphere-2025-5474
Preprint. Discussion started: 18 November 2025

$$\varphi(t^*) = e^{-\rho' \ln(1.8\,\tilde{s}\,t^*)^3} \quad (3)$$

in which $\rho' \equiv \frac{4\pi\rho}{3\alpha^3}$, where ρ is the density of recombination centres and α is a constant (Huntley, 2006; Kars et al., 2008).

To compute the athermal steady-state value of feldspar luminescence signals, $\tilde{n}_{ss}$, the following equation is used (Li and Li, 2008; King et al., 2016a):

$$\tilde{n}_{ss} = \int_{r'=0}^{\infty} \frac{3\,r'^2\,e^{-r'^3}}{1+\frac{D_0}{\dot{D}}\,\tilde{s}\,e^{-\rho'^{-\frac{1}{3}}r'}}\,dr' \quad (4)$$

where the dimensionless distance $r' \equiv \left\{\frac{4\pi\rho}{3}\right\}^{\frac{1}{3}} r$, with r the tunnelling distance from a trap to a recombination centre, and the probability that the nearest recombination centre is at a distance between r' and $r' + dr'$ is given by $p(r')dr' = 3r'^2 e^{-r'^3} dr'$ (Huntley, 2006).

2.2 Signal growth

Trapped-charge signals accumulate in response to the exposure of feldspar and quartz minerals to ionizing radiation. Various models have been proposed for luminescence and ESR signal growth. In the OSLThermo library, the single-saturating exponential (SSE; Apers et al., 1981) and general order kinetic (GOK; Guralnik et al., 2015b) growth functions have been implemented. In the ESRThermo library in addition to SSE and GOK, a linear (LIN) growth function has also been implemented for signals that do not appear to experience saturation (King et al., 2020).

In trapped-charge thermochronometry, the saturation ratio of the centre under investigation is usually considered, rather than the age, consequently, $\tilde{n}$ ratios are calculated for all of the signal growth fitting options with the exception of the LIN model, where *N*, the maximum possible trapped-charge concentration, cannot be constrained, and $\tilde{n}$ thus only represents the trapped-charge population. For this model, rather the total dose, D (Gy), accumulated, i.e., the equivalent dose, D_e (Gy), of the natural sample is considered.

The different dose response models are given below:

(i) Single saturating exponential (SSE) growth

$$\tilde{n}(t) = \varphi(t^*) \cdot A\left(1 - e^{-\frac{\dot{D}_{lab}\,t}{D_0}}\right) \quad (5)$$

where $\tilde{n}(t)$ is the ratio of trapped electrons at time t (s), A is a pre-exponential multiplier, $\dot{D}_{lab}$ (Gy·s^{-1}) is the laboratory dose rate and φ accounts for athermal detrapping (Eq. (2) and Eq. (3)). Note that athermal detrapping is only applicable for luminescence signals from feldspar and this term is not incorporated in the ESRThermo library. Single saturating exponential fits have been used previously to fit both luminescence (e.g., Herman et al., 2010) and ESR (e.g., Grün et al., 1999) thermochronometry data.

https://doi.org/10.5194/egusphere-2025-5474
Preprint. Discussion started: 18 November 2025

(ii) General order kinetic (GOK) growth

$$\tilde{n}(t) = \varphi(t^{*}) \cdot A\left(1 - \left(1 + \left(\frac{\dot{D}_{lab}}{D_0}\right) c\, t\right)\right)^{-\frac{1}{c}} \quad (6)$$

Where the kinetic order of trapping, α = c + 1 (Guralnik et al., 2015b). General order kinetic models have been used to fit both IRSL (e.g., Guralnik et al., 2015a; Lambert, 2018) and thermoluminescence data (Biswas et al., 2018).

(iii) Linear (LIN) growth

$$\tilde{n}(t) \approx D_e(t) = t\,\dot{D} \quad (7)$$

Linear growth has been used to describe the ESR response of the Al-centre within the context of ESR-thermochronometry (King et al., 2020).

2.3 Thermal signal loss

The thermal sensitivity of trapped-charge signals is well known (e.g., Aitken, 1985). The following models have been implemented in the OSLThermo and ESRThermo libraries: (i) the band-tail states model (BTS; Li and Li, 2013), (ii) the general order kinetics model (GOK; Guralnik et al., 2015a), and (iii) the Gaussian distribution model (GAUSS; Lambert, 2018). The mathematical basis of the models is described below:

(i) Band-tail states (BTS)

$$\frac{n(t)}{n(0)} = \varphi(t^{*}) \cdot \int_0^{E_t} P(E_b)\, e^{\left(-s\,t\,e^{-\frac{E_t - E_b}{k_B T}}\right)} dE_b \quad (8)$$

where E_t (eV) is the trap depth of the electron trap, and E_b (eV) is the depth of the band-tail state below the conduction band. The probability of thermally evicting electrons into band-tail states of energy in the range of $E_b + dE_b$, $P(E_b)\, dE_b$, is given by (Poolton et al., 2009; Li and Li, 2013):

$$P(E_b)\, dE_b = C\, e^{(-\frac{E_b}{E_u})} dE_b \quad (9)$$

where C is a pre-exponential multiplier and E_u (eV) is the width of the Urbach tail. King et al. (2016a; 2016c), Herman and King (2018), King et al. (2020), Bouscary and King (2022) and Ogata et al. (2022) used the BTS model to describe their multi-luminescence-thermochronometry data from feldspar minerals.

(ii) General order kinetics (GOK)

$$\frac{n(t)}{n(0)} = \varphi(t^{*}) \cdot \left[n(0)^{1-\beta} - (1-\beta)\, s\, t\, e^{-\frac{E_t}{k_B T}}\right]^{\frac{1}{1-\beta}} \quad (10)$$

https://doi.org/10.5194/egusphere-2025-5474
Preprint. Discussion started: 18 November 2025

Note that if the kinetic order, β, is fixed at 1 or 2, the model reverts to first-order or second-order kinetics respectively. Guralnik et al. (2015b) used GOK thermal decay to fit their infra-red stimulated luminescence thermochronometry for samples from the KTB borehole, whilst Biswas et al. (2018) and Stalder et al. (2022) used a similar approach to fit their thermoluminescence thermochronometry data. Wu et al. (2015) employed first-order kinetics to fit quartz luminescence data for samples from Taiwan, while Toyoda and Ikeya (1991) used second-order kinetics to describe the thermal decay of the ESR Al- and Ti-centres of quartz minerals, noting their potential for thermochronometry.

(iii) Gaussian distribution model (GAUSS)

The GAUSS distribution model assumes a Gaussian distribution of trap depths, with mean trap depth $\mu(E_t)$ (eV) and width $\sigma(E_t)$ (eV) (Lambert, 2018), with:

$$\frac{n(t)}{n(0)} = \varphi(t^*) \cdot \int_0^{E_a(max)} P_t(E_t)\, e^{\left(-s\,t\,e^{-\frac{E_t}{k_B T}}\right)} dE_t \tag{11}$$

where $E_a(max)$ is arbitrarily set to 9 eV, corresponding to the maximum optical bandgap for amorphous quartz (DiStefano and Eastman, 1971), and the probability of eviction $P_t(E_t)$ given by:

$$P_t(E_t) = \frac{1}{\sigma(E_t)\sqrt{2\pi}}\, e^{\left(-\frac{1}{2}\left(\frac{E_t-\mu(E_t)}{\sigma(E_t)}\right)^2\right)} \tag{12}$$

Lambert (2018) used the GAUSS model to describe thermal losses from the IRSL signals of feldspar minerals from the Mont Blanc massif, whilst King et al. (2020) and Bartz et al. (2024) used the GAUSS model to describe thermal signal losses from the ESR Al- and Ti-centres of quartz samples from Japan.

2.4 Data inversion

Using the kinetic parameters derived from fitting experimental data with the T-C models described above, it is possible to use the rate equation Eq. (1) to invert for a thermal history. For the luminescence of feldspar, the model must be integrated over the range of recombination centre distances *r'* and, for the BTS and GAUSS models, over the range of activation energies E_a described by Eq. (8) and Eq. (11) (where $E_a = E_t - E_b$ for the BTS model, and $E_a = E_t - \mu(E_t)$ for the GAUSS model). For quartz ESR data, as quartz minerals do not experience athermal fading, the third term on the right-hand side of the equation can be discarded. In this case, it is only necessary to integrate over the range of activation energies:

$$\frac{\mathrm{d}\tilde{n}}{\mathrm{d}t} = \frac{\dot{D}}{D_0}\,(1-\tilde{n})^{\alpha} - s\,\tilde{n}^{\beta}\, e^{\left(-\frac{E_t}{k_B T}\right)} \tag{13}$$

Finally for a non-saturating system exhibiting linear dose response, Eq. (14) is used:

$$\frac{\mathrm{d}\tilde{n}}{\mathrm{d}t} \approx \frac{\mathrm{d}D}{\mathrm{d}t} = \dot{D} - s\,D\, e^{\left(-\frac{E_t-\mu(E_t)}{k_B T}\right)} \tag{14}$$

https://doi.org/10.5194/egusphere-2025-5474
Preprint. Discussion started: 18 November 2025

3 Structure of OSLThermo and ESRThermo

The two libraries described here are structured in a similar manner (Table 1), that allows the input of partially processed trapped-charge data into MATLAB. Each library can be divided into two main parts: data fitting and inversion. Data fitting relates to the derivation of the kinetic parameters that describe signal growth and decay, and inversion to using these parameters to predict thermal histories from the natural trapped-charge concentrations of the sample under investigation (Table 1).

Table 1: Overview of the structure of the OSLThermo and ESRThermo libraries.

	Script name	*Description*	*Output*
Data fitting	OSLThermo/ ESRThermo	The main script that calls the other scripts, where the user selects the T-C models to use and which scripts to run (see Stage1 to Stage4b below).	Depends on the scripts that are run (see Stage1 to Stage4b below).
	Stage1_ExceltoStruct	Uploads the data from a pre-defined Excel spreadsheet format (see Fig. 2).	filename.mat containing structure, 'records', of the raw data
	Stage2a_Fitparameters	Fits the raw data with the selected T-C models to obtain kinetic parameters.	fitpar.mat containing structure, 'records.params', of the kinetic parameters
	Stage2b_PlotFit	Plots raw data with model fits.	Figures of the data fitting (see Fig. 1)
Inversion	Stage3a_Invesion	Inverts for a cooling history using the selected T-C models and output from Stage2a.	'Tt.mat', structure containing the inversion results
	Stage3b_PlotTt	Plots cooling inversion results.	Figures of the cooling inversion results (see Fig. 3)
	Stage4a_InversionExh	Inverts for exhumation rate using the selected T-C models and output from Stage2a.	'Zt.mat', structure containing the inversion results
	Stage4b_PlotExh	Plots exhumation inversion results.	Figures of the exhumation inversion results (see Fig. 4)

4 Experimental data

The OSLThermo and ESRThermo libraries are designed for the following three experimental data types but could be modified for different types of experimental data if required. (i) Luminescence or ESR dose response data measured in a regenerative dose protocol until saturation (except in the case of some ESR Al-centre signals that do not saturate at laboratory doses), i.e. the luminescence or ESR response to a range of laboratory irradiation doses including zero dose. The laboratory irradiation source dose rate ($Gy \cdot s^{-1}$) must be listed in the data input file, as well as the irradiation times (ks) (Fig. 2). (ii) Isothermal decay data for a minimum of one isothermal holding temperature, however, we strongly recommend including at least two isothermal holding temperatures. Using only one isothermal holding temperature often results on large and poorly constrained errors in the derived thermal kinetic parameters, whereas two or more temperatures significantly improve the accuracy and reliability of the fit. The isothermal holding temperatures (°C) must be listed in the data input file together with the isothermal holding times (ks) (Fig. 2). (iii) Anomalous fading data for feldspar luminescence data only. The fading time (ks), derived from the irradiation times and the time delay between irradiation and the start of the trapped-charge measurement, should be calculated

https://doi.org/10.5194/egusphere-2025-5474
Preprint. Discussion started: 18 November 2025

following Appendix F of Aitken (1985). These times can be directly extracted from the t* (hrs) values given in Analyst (see Duller, 2018).

The data format for the Excel data input file is shown in Fig. 2 for an example luminescence sample. The background subtracted integrated signals for each of the measurements (e.g., Lx/Tx values for luminescence) should be input into the Excel spreadsheet for each measurement point. Templates populated with the example data shown here are available for download from GitHub [*https://github.com/GeorginaKing/OSLThermo* & *https://github.com/GeorginaKing/ESRThermo*, "Data" folder]. Where fewer dose response, isothermal holding temperatures, or athermal fading data have been measured, the rows should be deleted and the values of 'nSAR' (number of measurements or aliquots measured for dose response curve measurements), 'nITH' (number of isothermal temperatures used in the isothermal holding experiment), and 'nFAD' (number of aliquots measured for athermal fading for IRSL) updated in the OSLThermo/ESRThermo script (see Section 5.1). This spreadsheet (Fig. 2) must be saved in the "Data" folder of the MATLAB library so that it can be called by the script *Stage1_ExcelToStruct* script (see Table 1 and further details below). It should then only be necessary for the user to modify the OSLThermo/ESRThermo script to read in, fit and invert their data.

	A	B	C	D	E	F	G	H	I	J	K	L	M	N	O
1	Sample		KRG104		Signal (type, temperature)		IRSL	225							
2	Natural T (°C)			10.0	2.0										
3	Natural Ḋ (Gy/ka)			6.16	0.83										
4	Lab calibration:														
5	T (°C)	15	t (ks)	Nat	0.000	0.250	0.500	1.500	3.000	6.000	12.000	24.000	48.000	0.000	0.250
6	Ḋ (Gy/s)	0.105	L_x/T_x	1.154	0.004	0.283	0.518	1.196	1.951	2.878	3.905	4.653	5.087	0.016	0.276
7	T (°C)	15	t (ks)	Nat	0.000	0.250	0.500	1.500	3.000	6.000	12.000	24.000	48.000	0.000	0.250
8	Ḋ (Gy/s)	0.105	L_x/T_x	1.778	0.006	0.281	0.519	1.219	1.928	3.009	3.949	4.623	5.294	0.020	0.289
9	T (°C)	15	t (ks)	Nat	0.000	0.250	0.500	1.500	3.000	6.000	12.000	24.000	48.000	0.000	0.250
10	Ḋ (Gy/s)	0.105	L_x/T_x	1.410	0.008	0.264	0.493	1.238	1.987	2.889	3.778	4.590	4.976	0.022	0.273
11	T (°C)	170	t (ks)	0.000	0.010	0.020	0.040	0.080	0.160	0.320	0.640	1.280	2.560	5.120	10.240
12	Ḋ (Gy/s)	0.105	L_x/T_x	0.928	0.931	0.916	0.915	0.917	0.901	0.906	0.924	0.895	0.879	0.825	0.833
13	T (°C)	190	t (ks)	0.000	0.010	0.020	0.040	0.080	0.160	0.320	0.640	1.280	2.560	5.120	10.240
14	Ḋ (Gy/s)	0.105	L_x/T_x	0.956	0.929	0.911	0.910	0.917	0.924	0.917	0.860	0.868	0.827	0.828	0.804
15	T (°C)	210	t (ks)	0.000	0.010	0.020	0.040	0.080	0.160	0.320	0.640	1.280	2.560	5.120	10.240
16	Ḋ (Gy/s)	0.105	L_x/T_x	0.952	0.901	0.912	0.923	0.911	0.886	0.903	0.874	0.830	0.793	0.771	0.742
17	T (°C)	230	t (ks)	0.000	0.010	0.020	0.040	0.080	0.160	0.320	0.640	1.280	2.560	5.120	10.240
18	Ḋ (Gy/s)	0.105	L_x/T_x	0.910	0.926	0.918	0.887	0.861	0.895	0.836	0.782	0.759	0.714	0.643	0.581
19	T (°C)	250	t (ks)	0.000	0.010	0.020	0.040	0.080	0.160	0.320	0.640	1.280	2.560	5.120	10.240
20	Ḋ (Gy/s)	0.105	L_x/T_x	0.908	0.896	0.888	0.860	0.824	0.799	0.792	0.754	0.687	0.613	0.533	0.444
21	T (°C)	300	t (ks)	0.000	0.010	0.020	0.040	0.080	0.160	0.320	0.640	1.280	2.560	5.120	10.240
22	Ḋ (Gy/s)	0.105	L_x/T_x	0.815	0.803	0.772	0.725	0.668	0.596	0.509	0.437	0.363	0.286	0.221	0.142
23	T (°C)	350	t (ks)	0.000	0.010	0.020	0.040	0.080	0.160	0.320	0.640				
24	Ḋ (Gy/s)	0.105	L_x/T_x	0.677	0.571	0.537	0.454	0.371	0.292	0.226	0.155				
25	T (°C)	15	t (ks)	1.156	17.546	23.576	35.626	59.706	1.159	10007.395	1.152	1.152			
26	Ḋ (Gy/s)	0.105	L_x/T_x	0.921	0.920	0.911	0.903	0.916	0.953	0.806	0.935	0.891			
27	T (°C)	15	t (ks)	1.156	19.051	25.085	37.134	61.218	1.159	10008.891	1.152				
28	Ḋ (Gy/s)	0.105	L_x/T_x	0.916	0.901	0.865	0.886	0.861	0.955	0.817	0.915				
29	T (°C)	15	t (ks)	1.156	20.556	26.593	38.646	62.734	1.159	10010.387	1.152				
30	Ḋ (Gy/s)	0.105	L_x/T_x	0.898	0.910	0.887	0.898	0.901	0.992	0.800	0.925				

Figure 2: Example Excel data input sheet for the OSLThermo library. Note that all of these data, except for the average surface temperature (that can be manually inputted in *Stage3a_Inversion* and *Stage4a_InversionExh* of the OSLThermo and ESRThermo scripts) and laboratory dose rates for the isothermal decay and fading measurements, are mandatory for the codes to run.

https://doi.org/10.5194/egusphere-2025-5474
Preprint. Discussion started: 18 November 2025

5 Running the code

The code comprises multiple stages, which are available on GitHub, and can be download at: https://github.com/GeorginaKing/OSLThermo & https://github.com/GeorginaKing/ESRThermo. Users will need both a MATLAB license and the Statistics and Machine Learning Toolbox to run the code. Example datasets are provided from King et al. (2016a) for OSLThermo and Bartz et al. (2024) for ESRThermo. The libraries contain the different MATLAB codes, with OSLThermo/ESRThermo being the main code/launcher that calls the other code stages that have been selected. Four folders are contained in the libraries: "Data" where the Excel files with the luminescence or ESR input data need to be placed, "Functions" which regroups the different functions used in the MATLAB codes, "ComputeData" where the computed data is output, and "Figures" where the computed figures are saved.

5.1 OSLThermo/ESRThermo

In OSLThermo/ESRThermo the user must provide the filename and select which models will be used to fit and invert the data ('SAR_fittype' and 'ITH_fittype'). The number of aliquots or measurements for the dose response curve, the number of isothermal temperatures investigated ('nITH'), and the number of aliquots or measurements for athermal fading ('nFAD', only for OSLThermo) must also be stated.

OSLThermo

```
%%% List of file names %%%
filenamevec = {'KRG104'};

%%% Number of measurements %%%
nSARvec = 3;   % number of aliquots measured for SAR
nITHvec = 7;   % number of isothermal decay temperatures
nFADvec = 3;   % number of aliquots measured for fading

%%% Select models %%%
SAR_ fittype = 1;  % 1=SSE; 2=GOK
ITH_ fittype  = 1;  % 1=BTS; 2=GOK; 3=GAUSS
```

ESRThermo

```
%%% List of file names %%%
filenamevec = {'TTY-A05'};

%%% Number of measurements %%%
nSARvec = 3;    % number of SAR measurements
nITHvec = 4;    % number of isothermal decay temperatures

%%% Select models %%%
SAR_fittype = 1;   % 1=SSE; 2=GOK; 3=LIN
ITH_fittype = 3;      % 2=GOK; 3=GAUSS
```

The user then selects which codes should be run for that particular sample, e.g., *Stage1_ExcelToStruct*, *Stage 2a_Fitparameters*, etc. Once a code has been run for a sample, the output is saved (see Table 1), so it is not necessary to run the code again unless the raw data have changed, or the data should be fitted with a different model.

5.2 Stage1_ExcelToStruct

This function imports the Excel data, stored in the subfolder "Data", into MATLAB and creates a MATLAB structure called 'records' that is called in *Stage2a_Fitparameters*:

OSLThermo

```
run Stage1_ExcelToStruct
```

ESRThermo

```
run Stage1_ExcelToStruct
```

https://doi.org/10.5194/egusphere-2025-5474
Preprint. Discussion started: 18 November 2025


```
>> records =
1×4 struct array with fields
        id: 'KRG104 IRSL225'
        typeMeasurement: 'IRSL'
        typeSignal: 225
        params: [1×1 struct]
        rawdata: [1×13 struct]

>> records.params =
struct with fields:
        natT: [10 2]
        natDdot: [1.9533e-10, 2.62693e-11]

>> records.rawdata =
1×13 struct array with fields:
        T
        labDdot
        t
        L
```

```
>> records =
1x2 struct array with fields:
        id: 'TTY-A05-Al'
        typeMeasurement: 'ESR'
        typeSignal: 'Al-centre'
        params: [1×1 struct]
        rawdata: [1×7 struct]

>> records.params =
struct with fields:
        natT: [10 5]
        natDdot: [1.2406e-10 1.1725e-11]

>> records.rawdata =
1×7 struct array with fields:
        T
        labDdot
        t
        ESR
```

This structure is saved as a .mat file in the subfolder "ComputeData", with the name *filename.mat*, and can be accessed without running *Stage1_ExcelToStruct* again. If multiple sheets are present in the Excel file, 'records' will comprise multiple datasets, which can be accessed separately by inputting records(i) where i is the record number, into the MATLAB Command Window. The different rows of rawdata, j can also be accessed directly, for example to access the duration of dose/isothermal annealing time (Table 2), one can input *records(i).rawdata(j).t* into the command line.

Table 2: Variable names and description of data stored in the MATLAB structure 'records' after running *Stage1_ExcelToStruct*.

Excel ID	MATLAB ID	Description
Sheet name	records(i).id	Excel sheet name
Type of measurement	records(i).typeMeasurement	Type of measurement (IRSL, ESR)
Type of signal	records(i).typeSignal	Type of signal (temperature of IRSL (°C), or ESR defect)
Natural T (°C)	records(i).params.natT	Natural temperature (°C)
Natural $\dot{D}$ (Gy·s^{-1})	records(i).params.natDdot	Natural environmental dose rate (Gy·s^{-1})
T (°C)	records(i).rawdata(j).T	Measurement temperature (°C)
$\dot{D}$ (Gy·s^{-1})	records(i).rawdata(j).labDdot	Instrument dose rate (Gy·s^{-1})
t (ks)	records(i).rawdata(j).t	Duration of dose/isothermal annealing (ks)
Lx/Tx	records(i).rawdata(j).L	Luminescence data *(OSLThermo only)*
ESR	records(i).rawdata(j).ESR	ESR data *(ESRThermo only)*

https://doi.org/10.5194/egusphere-2025-5474
Preprint. Discussion started: 18 November 2025

5.3 Stage2a_Fitparameters

This script calls *filename.mat*, created by *Stage1a_ExcelToStruct*, and fits the raw data using the T-C models specified in the OSLThermo/ESRThermo script. The dose response and athermal fading data are fitted independently for each aliquot/measurement to account for individual laboratory dose rates and varying maximum trapped-charge signal values. The kinetic parameters output by the script are averaged per signal type across the different aliquots/measurements, and depend on the T-C models used. They are summarised in Table 3 per T-C model. In the MATLAB codes, these parameters are stored in the structure 'records' as 'records.params', and are exported in an Excel table. In addition to the kinetic parameters, the modelled data fits are stored in the structure 'records' as 'records.plot' for plotting in *Stage2b_PlotFit*.

OSLThermo

```
>> records =
1 x 4 struct array with fields:
        id: 'KRG104 IR225'
        typeMeasurement: 'IRSL'
        typeSignal: 225
        params: [1×1 struct]
        rawdata: [1×13 struct]
        SAR_model: 'SSE'
        ITH_model: 'BTS'
        plot: [1×1 struct]

>> records.params =
struct with fields:
        natT: [10, 2]
        natDdot: [1.9533e-10, 2.6269e-11]
        rhop10: [-5.6606, 0.0573]
        g2d: [2.6846, 0.3351]
        D0: [708.8781, 30.9929]
        GOK_a: [NaN, NaN]
        Et: [1.3831, 0.0443]
        Eu: [0.1244, 0.0071]
        GOK_b: [NaN, NaN]
        sigmaEt: [NaN, NaN]
        s10: [8.0616, 0.3714]
        NatFadedDe: [386.9116, 82.5055]
        NatFadedD0: [687.1585]
        AgeOSL: [62.7696, 15.8248]
        maxAgeOSL: [222.9586]
        nNnat: [0.2391, 0.0497]
        nNss: [0.5555, 0.0441]
```

ESRThermo

```
>> records =
1 x 2 struct array with fields:
        id: 'TTY-A05-Al'
        typeMeasurement: 'ESR'
        typeSignal: 'Al-centre'
        params: [1×1 struct]
        rawdata: [1×7 struct]
        SAR_model: 'SSE'
        ITH_model: 'GAUSS'
        plot: [1×1 struct]

>> records.params =
struct with fields:
        natT: [10, 5]
        natDdot: [1.2406e-10, 1.1725e-11]
        De: [1.5093e+03, 48.2475]
        D0: [1.1030e+04, 965.1034]
        GOK_a: [NaN, NaN]
        s10: [13.5306, 0.6237]
        Et: [1.5338, 0.0561]
        GOK_b: [NaN, NaN]
        sigmaEt: [0.0897, 0.0049]
        AgeESR: [385.5232, 38.4629]
        nNnat: [0.1279, 0.0041]
```

https://doi.org/10.5194/egusphere-2025-5474
Preprint. Discussion started: 18 November 2025

Table 3: Description of the parameters output by *Stage2a_Fitparameters* and stored in 'records.params', depending on the T-C models selected. Additional useful values are calculated in the codes but are not extensively discussed in this manuscript, which focuses on the key parameters used in the different scripts.

Parameter	OSLThermo MATLAB ID	ESRThermo MATLAB ID
Environmental parameters		
T_{nat} (°C) – average surface temperature	natT	natT
$\dot{D}$ (Gy·s^{-1}) – natural environmental dose rate	natDdot	natDdot
Athermal detrapping model (OSLThermo script only)		
ρ' (-) – recombination centre density	rhop10	-
g_{2d} (%/dec.) – fading rate normalised to 2 days	g2d	-
$\tilde{n}_{ss}$ (-) – athermal steady-state signal (fading corrected)	nNss	-
Trapping models		
SSE		
$\tilde{n}_{nat}$ (-) – natural signal	nNnat *	nNnat
D_e (Gy) – equivalent dose	NatFadedDe*	De
D_0 (Gy) – characteristic dose of saturation	D0 *	D0
D_{0_nat} (Gy) – D_0 for the natural faded signal	NatFadedD0 *	-
GOK		
$\tilde{n}_{nat}$ (-) – natural signal	nNnat *	nNnat
D_e (Gy) – equivalent dose	NatFadedDe*	De
D_0 (Gy) – characteristic dose of saturation	D0 *	D0
D_{0_nat} (Gy) – D_0 for the natural faded signal	NatFadedD0 *	-
a (-) – kinetic order of trapping	GOK_a	GOK_a
LIN		
D_e (Gy) – equivalent dose	-	De
Detrapping models		
BTS		
E_t (eV) – trap depth	Et	-
E_u (eV) – Urbach width	Eu	-
s (s^{-1}) – frequency factor	s10	-
GOK		
E_t (eV) – trap depth	Et	Et
b (-) – kinetic order of detrapping	GOK_b	GOK_b
s (s^{-1}) – frequency factor	s10	s10
GAUSS		
$\mu(E_t)$ (eV) – mean trap depth	Et	Et
$\sigma(E_t)$ (eV) – standard deviation of trap depth (width)	sigmaEt	sigmaEt
s (s^{-1}) – frequency factor	s10	s10
Ages		
Age (ka) – Apparent age	AgeOSL *	AgeESR
Age_{max} (ka) – Max. age, calculated for $2.D_{0\_nat}$	maxAgeOSL *	-

Note: for the OSLThermo script, all data with an asterisk (*) are fading corrected values.

https://doi.org/10.5194/egusphere-2025-5474
Preprint. Discussion started: 18 November 2025

5.4 Stage2b_PlotFit

Stage2b_PlotFit calls *filename.mat*, created in *Stage1_ExcelToStruct* and updated in *Stage2a_Fitparameters*, and produces plots of the raw data and model fits. In the OSLThermo library, the output of the Huntley (2006) model to test for luminescence signal saturation due to anomalous fading (Kars et al., 2008; Valla et al., 2016) is also plotted ($\tilde{n}_{ss}$ vs. $\tilde{n}_{nat}$; Fig. 1D). The figures produced for the two example datasets are shown in Fig. 1 and are automatically saved as either .png, .svg, or .eps files to the subfolder “Figures”. Whilst it is not necessary to run *Stage2b_PlotFit* prior to running *Stage3a_Inversion* as no additional data fitting occurs in the script, it is good practice to make a visual inspection of the quality of data fitting before proceeding to the data inversion.

5.5 Stage3a_Inversion

Stage3a_Inversion inverts trapped-charge data for rock cooling history, using the parameters calculated in *Stage2a_Fitparameters*, assuming monotonic cooling. All the data from a single Excel file are inverted together, for example different temperature IRSL data saved on different sheets of the same Excel file (Fig. 2). Note that the same T-C models used for fitting the data, must be used for the inversion. For OSLThermo, default parameters are setup for the model to run for 1 Myr assuming cooling from Tmax = 150 °C to Tmin = 10 ± 5 °C using niter = 5000 iterations; and for ESRThermo, the model is setup to run for 5 Myr assuming cooling from Tmax = 200 °C to Tmin = 10 ± 5 °C using niter = 5000 iterations. These conditions can be changed by editing the following lines of code:

```
%%% Model parameters
Tmax = 150;                      % maximum temperature in (°C)
Tsurf = 10;   TsurfErr = 5;      % average modern surface or sample temperature in (°C), and uncertainty
tmax = 1;                        % maximum time in (Ma)
tmin = 0;                        % minimum time in (Ma)
nstep = 501;                     % discretisation of the model in time
time = linspace(tmin,tmax,nstep);

%%% Number of iterations
niter = 5000;                    % number of random realisations / Monte Carlo iterations
```

More iterations will require a longer computational time. The principles of the inversion are fully described in King et al. (2016a) and King et al. (2020) and are outlined briefly here. Random monotonic cooling histories are generated, and for each history, the accumulation of trapped-charge is calculated using Eq. (1) (Fig. 3B-E, H) and the sample specific kinetic parameters determined in *Stage2a_Fitparameters*. The quality of each model fit to the natural measured data is assessed by comparing the final modelled $\tilde{n}_{mod}$ value, $\tilde{n}_{mod,f}$ (i.e. the value calculated after 1 Ma for OSLThermo, and 5 Ma for ESRThermo) to the natural measured value $\tilde{n}_{nat}$ using a misfit function, M (Eq. (15); Fig. 3F, I). This function has been updated since King et al. (2016a) following Wheelock et al. (2015), and as described by King et al. (2020) and Biswas et al. (2020):

https://doi.org/10.5194/egusphere-2025-5474
Preprint. Discussion started: 18 November 2025

$$M = \left(\frac{1}{2}\frac{\tilde{n}_{nat}}{\sigma\tilde{n}_{nat}}\log\left(\frac{\tilde{n}_{nat}}{\tilde{n}_{mod,f}}\right)\right)^2 \quad (15)$$

where, $\sigma\tilde{n}_{nat}$ is the uncertainty on $\tilde{n}_{nat}$. The value of $\sigma\tilde{n}_{nat}$ can be determined either from the measured uncertainty or set arbitrarily, for example as 5 or 10% of $\tilde{n}_{nat}$, or as a fixed value, e.g., 0.05.

```
%%% Redefine uncertainties (OPTIONAL)
% snNnat(snNnat<0.05) = 0.05;                  % set the uncertainty to 0.05 when it is <0.05
% snNnat(snNnat./nNnat<0.05) = 0.05*nNNnat;    % set the uncertainty to 5% of ñnat when it is <5%
snNnat = 0.05*nNnat;                           % set the uncertainty on ñnat to 5% of ñnat
```

The results of the inversion (time-temperature paths, $\tilde{n}_{mod}$ vectors, and misfit values) are saved in a MATLAB structure called 'Tt', which is saved in the "ComputeData" subfolder.

OSLThermo

```
>> Tt =
struct with fields:
      misfit: [5000×1 double]
      time: [5000×501 double]
      temp: [5000×501 double]
      nNmod: [5000×501×4 double]
      nNnat: [0.0866 ; 0.1577 ; 0.1802 ; 0.2391]
      snNnat: [0.0043 ; 0.0079 ; 0.0090 ; 0.0120]
      AgeOSL: c1 [81.37 ; 57.61 ; 56.93 ; 62.77]
              c2 [15.39 ; 16.01 ; 14.02 ; 15.82]
      maxAgeOSL: [236.95 ; 219.70 ; 243.70 ; 222.96]
      TypeMeasurement: {'IRSL' 'IRSL' 'IRSL' 'IRSL'}
      TypeSignal: [50 100 150 225]
```

ESRThermo

```
>> Tt =
struct with fields:
      misfit: [5000×1 double]
      time: [5000×501 double]
      temp: [5000×501 double]
      nNmod: [5000×501×2 double]
      nNnat: [0.1279 ; 0.4754]
      snNnat: [0.0064 ; 0.0238]
      AgeESR: c1 [385.52 ; 508.76]
              c2 [38.46 ; 50.24]
      TypeMeasurement: {'ESR' 'ESR'}
      TypeSignal: {'Al-centre' 'Ti-centre'}
```

In addition to investigating rock cooling, it is also possible to investigate isothermal histories or specific thermal histories by replacing the random cooling history generated using the randpathAD function with a specific time-temperature history.

5.6 Stage3b_PlotTt

Stage3b_PlotTt uses the output from *Stage3a_Inversion* and computes a probability density function from the inversion results. The likelihood, L, of a particular cooling history is computed from the misfit scores:

$$L = e^{-M} \quad (16)$$

and normalised by the maximum likelihood (L_{max}), before these values are passed through a rejection algorithm whereby values of L are contrasted with a random number between 0 and 1, and only values that are greater than the random number are retained (Tarantola, 2005). The cooling histories retained are then used to compute a probability density function. This is done by dividing the time-temperature space into equal-size cells and calculating the number of time-temperature paths passing through each cell. The results of inverting the example datasets are shown in Fig. 3.

https://doi.org/10.5194/egusphere-2025-5474
Preprint. Discussion started: 18 November 2025

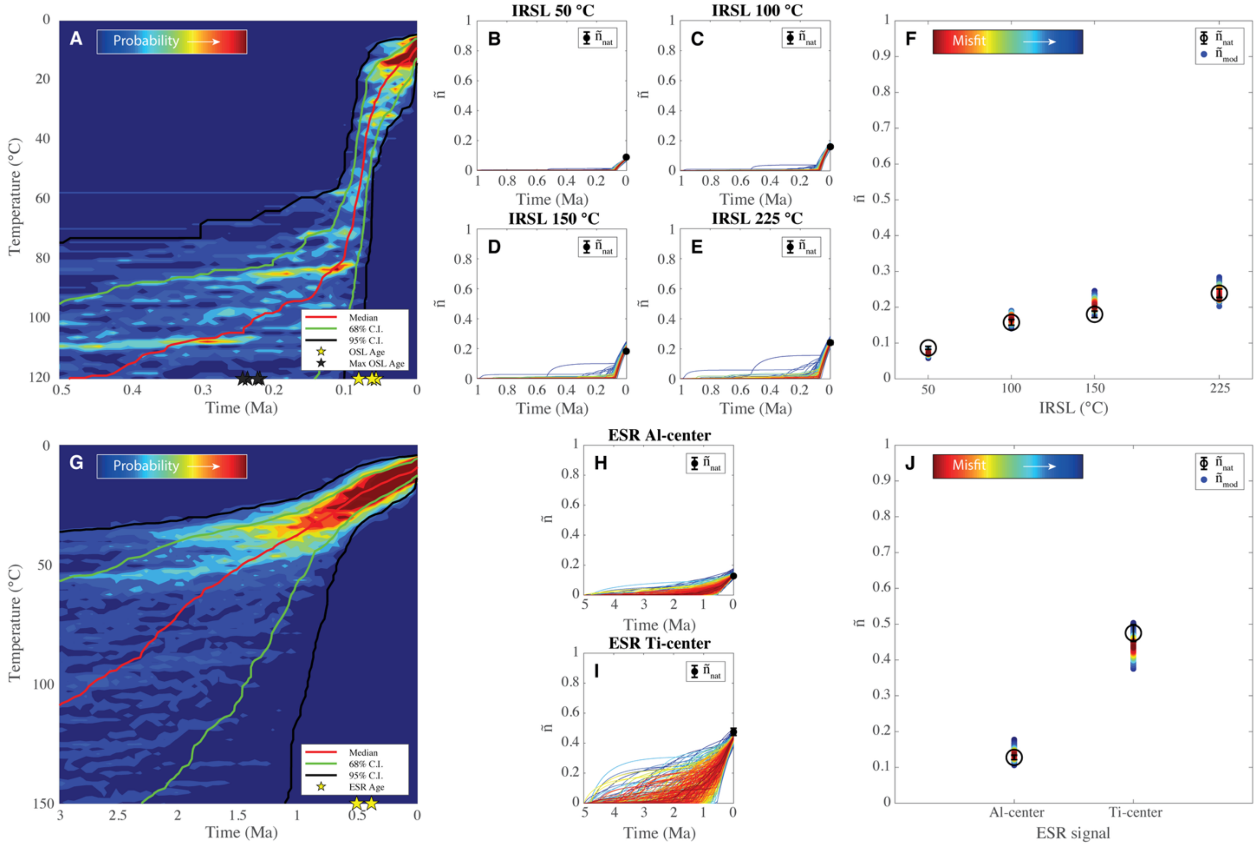

Figure 3: Cooling history inversion results for IRSL and ESR data from the two Japanese Alps example samples (King et al, 2020; Bartz et al., 2024). Probability density function of the accepted time-temperature history (cooling path) (A) for all four IRSL signals of sample KRG104 and (G) for the Al-centre and Ti-centre of sample TTY-A05; modelled signal accumulation (B-E, H-I) and misfit between measured and modelled values (F, J) for the time-temperature paths that passed the rejection algorithm. In (A, G), the red line is the median cooling path, and the green and black lines are the 68% and 95% confidence intervals, respectively.

5.7 Stage4a_InversionExh

Stage4a_InversionExh allows the inversion of trapped-charge data for an exhumation history; the approach is fully described in Biswas et al. (2018) and is only briefly explained here. In this script, random time-temperature histories are first generated over a specified time-period and depth. Rock cooling histories for each time-depth path are then computed using the 1D heat-transfer equation, and the accumulation of trapped-charge is calculated using Eq. (1) and the sample-specific kinetic parameters determined in *Stage2a_Fitparameters*. As for *Stage3a_Inversion*, the quality of each model fit to the natural measured data is assessed by comparing the final modelled $\tilde{n}$ value, $\tilde{n}_{mod,f}$, using Eq. (15).

https://doi.org/10.5194/egusphere-2025-5474
Preprint. Discussion started: 18 November 2025

The model is set-up to run over the last 5 Ma ('tmax') over a depth of 15 km ('Lz') with an initial geothermal gradient of 30 °C·km^{-1} ('G'). The thermal diffusivity ('kappa0'), number of iterations ('niter') and discretization of the model ('nstep') can also be modified. This code is more computationally expensive than *Stage3a_Inversion* and it requires more iterations to yield a similar number of accepted paths.

```
%%% Physics
kappa0 = 30;                      % thermal diffusivity (km²·Myr⁻¹)
Lz    = 15;                       % depth (km), use 25 km for high temperature thermochronometers
G     = 30;                       % initial temperature gradient (°C·km⁻¹)
Tsurf=10; TsurfErr=5;             % surface temperature (°C) and its uncertainty

%%% Numerics: discretization, time steps and plotting frequency
nz    = 31;                       % number of nodes
dz    = Lz/(nz-1);                % node size (km)

%%% Choose the depth time history (i.e. exhumation rate history)
Zmax    = Lz;                     % maximum depth in (km)
Zmin    = 0;                      % surface, i.e. Z=0 km
tmax    = 5;                      % time in Ma (today)
tmin    = 0;
nstep   = 6000;                   % timestep, to ensure high resolution over the timescale
dt      = (tmax-tmin)./(nstep-1); % calculate timestep, dt (Myr)
tvec    = (tmin:dt:tmax);         % create time vector

%%% Number of iterations
niter   = 100000;                 % number of iterations
```

5.8 Stage4b_PlotZt

Stage4b_PlotZt plots the inversion results from *Stage4a_InversionExh*. The depth and time-period of interest are defined in the plotting script (and are usually smaller than the modelled domain), as is the matrix resolution for computing the exhumation history. As the geothermal gradient (G) evolves throughout the inversion, a final geothermal gradient that is unfeasibly high may be obtained. For this reason, a threshold value can be defined (G_cut) to exclude results with a final $G > G\_cut$ (see Stalder et al., 2022 for a discussion). G_cut is set to 100 °C·km^{-1} in the code, but this value can be modified.

```
%%% Define parameters for plotting
DoI   = 2;                        % depth of interest, last xx (km)
ToI   = 0.3;                      % time of interest, last xx (Ma)
G_cut = 100;                      % cut-off for geothermal gradient (°C·km⁻¹)
time_window = ToI;                % restrict to a time-window of interest for plotting

%%% Resolution of matrix
nAvM = 1200;                      % temporal dt = ToI/nAvM and spatial dZ = DoI/nAvM resolutions
resampling = 100;                 % how many times median is resampled (min. 100)
nb_path    = 0.10;                % number of resampled paths in % of total accepted paths (min. 10% = 0.10)
vel_interval = 10;                % define velocity smoothing interval in (kyr)
```

https://doi.org/10.5194/egusphere-2025-5474
Preprint. Discussion started: 18 November 2025

This script produces a range of figures, including a probability density function of time-depth for the accepted paths (Fig. 4A, D), as well as a comparison between modelled ($\tilde{n}_{mod}$) and measured ($\tilde{n}_{nat}$) values, and in the case of luminescence data, the predicted field saturation values, $\tilde{n}_{ss}$, for the sample under investigation (Fig. 4B, E). It also produces a figure showing the time series of the modelled exhumation history in linear and log space (Fig. 4C, D).

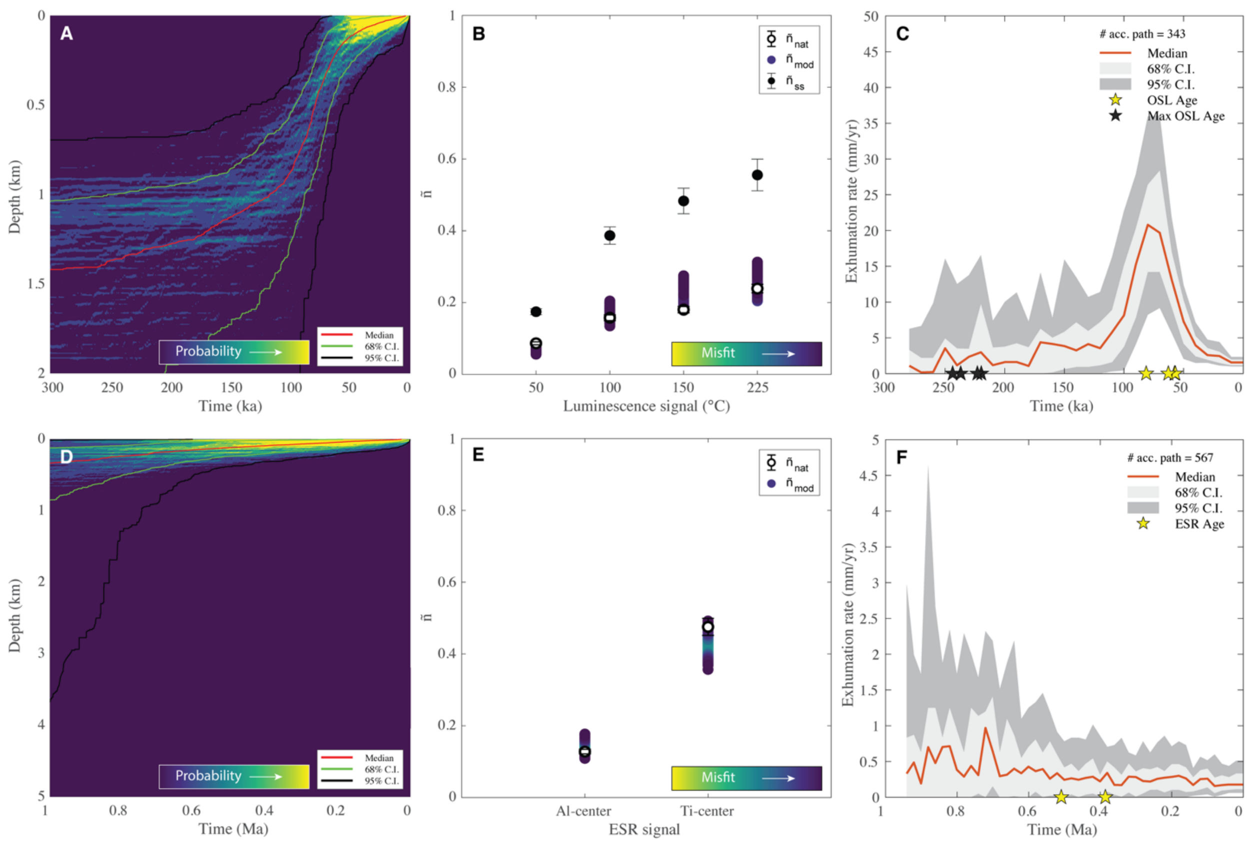

Figure 4: Exhumation rate inversion results for IRSL (A-C) and ESR (D- F) data following 10,000 iterations. Probability density function of the accepted time-depth history (exhumation path) (A) for all four IRSL signals of sample KRG104 and (D) for the ESR Al- and Ti-centre of sample TTY-A05; misfit between measured and modelled values (B, E) and time-series of exhumation rate changes (C, F) plotted in linear space. In (A, D), the red line is the median cooling path, and the green and black lines are the 68% and 95% confidence intervals respectively.

6 Outlook

We hope that by sharing the codes that we have developed for the modelling of trapped-charge thermochronometry data for feldspar OSL and quartz ESR, we will encourage broader application and further development of trapped-charge

https://doi.org/10.5194/egusphere-2025-5474
Preprint. Discussion started: 18 November 2025

thermochronometry and thermometry techniques. The codes can easily be adapted for other trapped-charge signals, such as quartz OSL or thermoluminescence. We will continue to update the OSLThermo and ESRThermo libraries as new T-C models emerge and as the trapped-charge community advances efforts to improve thermochronometric analysis, for example, by incorporating averaging thermal kinetic parameters (Bouscary and King, 2024), enabling more complex thermal histories (e.g., reheating), or integrating trapped-charge data with other thermochronometric systems. By fostering open-source development and collaboration, we aim to support the growth and integration of trapped-charge thermochronometry within the broader thermochronological and geochronological community.

Codes are available for download on GitHub: *https://github.com/GeorginaKing/OSLThermo* for luminescence thermochronometry & *https://github.com/GeorginaKing/ESRThermo* for ESR thermochronometry.

Author contributions

CB, GEK, MB, AD, BG, and FH contributed to the conceptualization and methodological design of the study. Data curation was performed by CB and GEK, while formal analyses were carried out by CB, GEK, MB, LB, AD, BG, FH, NS, and VV. The investigation and methodological implementation involved almost all authors (CB, GEK, MKB, MB, RHB, AD, BG, FH, UN, PGV, VV, and XW), with validation contributions from CB, GEK, MKB, MB, BG, FH, and XW. Software development and implementation were undertaken by CB, GEK, MKB, MB, RHB, AD, BG, FH, UN, and VV. Supervision was led by GEK, FH, and BG. Project administration and resource provision were coordinated by GEK and FH, and funding was acquired by CB, GEK, and FH. The original manuscript draft was written by CB and GEK, and all authors contributed to the review, editing, or validation of the final version.

Code and Data availability

The codes used in this study are publicly available on GitHub: for OSL thermochronometry on feldspar at https://github.com/GeorginaKing/OSLThermo and for ESR thermochronometry on quartz at https://github.com/GeorginaKing/ESRThermo. For each code, the Excel input file corresponding to the sample analysed in this manuscript is provided, allowing direct reproduction of the results.

Competing interests

One of the co-authors serves on the Editorial Board of the journal *GChron*.

Acknowledgements

This project has received funding from the European Research Council (ERC) under the European Union's Horizon 2020 research and innovation programme (Grant agreement No. 85164), as well as from the Swiss National Science Foundation (PZ00P2_167960 awarded to GEK, PP00P2-38956 awarded to FH, and P500PN_217747 awarded to CB). We are very grateful to Renske Lambert and Aleksandar Licul for their contributions to the development of the codes.

References

Aitken, M.J.: Thermoluminescence dating, Academic Press, Harcourt Brace Jovanovich Publishers, 351 pp. ISBN 0-12-046381-4, 1985

Apers, D., Debuyst, R., de Canniere, P., Dejehet, F., and Lombard, E.: A criticism of the dating by electronic paramagnetic resonance (ESR) of the stalagmite floors of the Caune de l'Arago at Tautavel, in Absolute Dating and Isotope Analyses in Prehistory, Methods and Limits, edited by de Lumley, H., and Lebeyrie, J., Paris, CNRS, 533-550, ISSN 0315-0941, 1981.

Bartz, M., King, G.E., Bernard, M., Herman, F., Wen, X., Sueoka, S., Tsukamoto, S., Braun, J., and Tagami, T.: The impact of climate on relief in the northern Japanese Alps within the past 1 Myr – The case of the Tateyama mountains, EPSL, 644, 118830, https://doi.org/10.1016/j.epsl.2024.118830, 2024.

Biswas, R.H., Herman, F., King, G.E., and Braun, J.: Thermoluminescence of feldspar as a multi-thermochronometer to constrain the temporal variation of rock exhumation in the recent past, EPSL, 495, 56-68, https://doi.org/10.1016/j.epsl.2018.04.030, 2018.

Biswas, R.H., Herman, F., King, G.E., Lehmann, B., and Singhvi, A.K.: Surface paleothermometry using low-temperature thermoluminescence of feldspar, Clim. Past, 16(6), 2075-2093, https://doi.org/10.5194/cp-16-2075-2020, 2020.

Bouscary, C., and King, G.E.: Luminescence thermochronometry of feldspar minerals: Optimisation of measurement conditions for the derivation of thermal kinetic parameters using isothermal holding experiments, Quat. Geochronol., 67, 101240, https://doi.org/10.1016/j.quageo.2021.101240, 2022.

Bouscary, C., King, G.E., Grujic, D., Lavé, J., Almeida, R., Hetényi, G., and Herman, F.: Sustained deformation across the Sub-Himalayas since 200 ka, Geology, 52(1), 72-76, https://doi.org/10.1130/G51656.1, 2024.

Bouscary, C., and King, G.E.: Exploring the use of averaged thermal kinetic parameters in luminescence thermochronometry, Radiat. Meas., 176, 107215, https://doi.org/10.1016/j.radmeas.2024.107215, 2024.

Brown, N.D., Rhodes, E.J., and Harrison, T.M.: Using thermoluminescence signals from feldspars for low-temperature thermochronology, Quat. Geochronol., 42, 31-41, https://doi.org/10.1016/j.quageo.2017.07.006, 2017.

DiStefano, T.H., and Eastman, D.E.: The band edge of amorphous SiO2 by photoinjection and photoconductivity measurements, Solid State Commun., 9(24), 2259-2261, https://doi.org/10.1016/0038-1098(71)90643-0, 1971.

Fang, F., and Grün, R.: ESR thermochronometry of Al and Ti centres in quartz: A case study of the Fergusons Hill-1 borehole from the Otway Basin, Australia, Radiat. Meas., 139, 106447, https://doi.org/10.1016/j.radmeas.2020.106447, 2020.

Grün, R., Tani, A., Gurbanov, A., Koshchug, D., Williams, I., and Braun, J.: A new method for the estimation of cooling and denudation rates using paramagnetic centers in quartz: A case study on the Eldzhurtinskiy Granite, Caucasus, J. Geophys. Res.: Solid Earth, 104(B8), 17531-17549, https://doi.org/10.1029/1999JB900173, 1999.

Guralnik, B., Jain, M., Herman, F., Ankjærgaard, C., Murray, A.S., Valla, P.G., Preusser, F., King, G.E., Chen, R., Lowick, S.E., and Kook, M.: OSL-thermochronometry of feldspar from the KTB borehole, Germany, EPSL, 423, 232-243, https://doi.org/10.1016/j.epsl.2015.04.032, 2015a.

Guralnik, B., Li, B., Jain, M., Chen, R., Paris, R.B., Murray, A.S., Li, S.H., Pagonis, V., Valla, P.G., and Herman, F.: Radiation-induced growth and isothermal decay of infrared-stimulated luminescence from feldspar, Radiat. Meas., 81, 224-231, https://doi.org/10.1016/j.radmeas.2015.02.011, 2015b.

Guralnik, B., and Sohbati, R.: Fundamentals of luminescence photo-and thermochronometry, in Advances in Physics and Applications of Optically and Thermally Stimulated Luminescence, Chen, R., and Pagonis, V., 399-437, https://doi.org/10.1142/q0172, 2019.

Herman, F., Rhodes, E.J., Braun, J., and Heiniger, L.: Uniform erosion rates and relief amplitude during glacial cycles in the Southern Alps of New Zealand, as revealed from OSL-thermochronology, EPSL, 297(1-2), 183-189, https://doi.org/10.1016/j.epsl.2010.06.019, 2010.

Herman, F., and King, G.E.: Luminescence thermochronometry: Investigating the link between mountain erosion, tectonics and climate, Elements, 14(1), 33-38, https://doi.org/10.2138/gselements.14.1.33, 2018.

Houtermans, F., Jager, E., Schon, M., and Staufer, H.: Measurements of the thermoluminescence as a means to investigate the thermal and radiation history of the natural minerals and rocks, Ann. Phys, 20, 283, https://doi.org/10.1002/andp.19574550129, 1957.

Huntley, D.J.: An explanation of the power-law decay of luminescence, J. Phys.: Condens. Matter, 18(4), 1359, https://doi.org/10.1088/0953-8984/18/4/020, 2006.

Kars, R.H., Wallinga, J., and Cohen, K.M.: A new approach towards anomalous fading correction for feldspar IRSL dating—tests on samples in field saturation, Radiat. Meas., 43(2-6), 786-790, https://doi.org/10.1016/j.radmeas.2008.01.021, 2008.

King, G.E., Herman, F., Lambert, R., Valla, P.G., and Guralnik, B.: Multi-OSL-thermochronometry of feldspar. Quat. Geochronol., 33, 76-87, https://doi.org/10.1016/j.quageo.2016.01.004, 2016a.

King, G.E., Guralnik, B., Valla, P.G., and Herman, F.: Trapped-charge thermochronometry and thermometry: A status review, Chem. Geol., 446, 3-17, https://doi.org/10.1016/j.chemgeo.2016.08.023, 2016b.

King, G.E., Herman, F., and Guralnik, B.: Northward migration of the eastern Himalayan syntaxis revealed by OSL thermochronometry, Science, 353(6301), 800-804, https:doi.org/10.1126/science.aaf2637, 2016c.

King, G.E., Tsukamoto, S., Herman, F., Biswas, R.H., Sueoka, S., and Tagami, T.: Electron spin resonance (ESR) thermochronometry of the Hida range of the Japanese Alps: validation and future potential, GChron, 2(1), 1-15, https://doi.org/10.5194/gchron-2-1-2020, 2020.

King, G.E., Ahadi, F., Sueoka, S., Herman, F., Anderson, L., Gautheron, C., Tsukamoto, S., Stalder, N., Biswas, R.H., Fox, M., Delpech, G., Schwartz, S., and Tagami, T.: Eustatic change modulates exhumation in the Japanese Alps, Geology, 51(2), 131-135, https://doi.org/10.1130/G50599.1, 2023.

Lambert, R.: Investigating thermal decay in K-feldspar for the application of IRSL thermochronometry on the Mont Blanc massif. Ph.D. thesis, Faculty of Geosciences and Environment, University of Lausanne, Switzerland, 154 pp., 2018.

Li, B., and Li, S.H.: Investigations of the dose-dependent anomalous fading rate of feldspar from sediments, J. Phys. D: Appl. Phys., 41(22), 225502, https//doi.org/10.1088/0022-3727/41/22/225502, 2008.

Li, B., and Li, S.H.: The effect of band-tail states on the thermal stability of the infrared stimulated luminescence from K-feldspar, J. Lumin., 136, 5-10, https://doi.org/10.1016/j.jlumin.2012.08.043, 2013.

Murray, A.S., and Wintle, A.G.: Luminescence dating of quartz using an improved single-aliquot regenerative-dose protocol, Radiat. Meas., 32(1), 57-73, https://doi.org/10.1016/S1350-4487(99)00253-X, 2000.

Ogata, M., King, G.E., Herman, F., and Sueoka, S.: Reconstructing the thermal structure of shallow crust in the Tono region using multi-OSL-thermometry of K-feldspar from deep borehole core, EPSL, 591, 117607, https://doi.org/10.1016/j.epsl.2022.117607, 2022.

Poolton, N.R.J., Kars, R.H., Wallinga, J., and Bos, A.J.J.: Direct evidence for the participation of band-tails and excited-state tunnelling in the luminescence of irradiated feldspars, J. Phys.: Condens. Matter, 21(48), 485505, http://doi.org/10.1088/0953-8984/21/48/485505, 2009.

Prokein, J., and Wagner, G.A.: Analysis of thermoluminescent glow peaks in quartz derived from the KTB-drill hole, Radiat. Meas., 23(1), 85-94, https://doi.org/10.1016/1350-4487(94)90026-4, 1994.

Ronca, L.B., and Zeller, E.J.: Thermoluminescence as a function of climate and temperature, Am. J. Sci., 263(5), 416-428, https://doi.org/10.2475/ajs.263.5.416, 1965.

Stalder, N.F., Biswas, R.H., and Herman, F.: Maximized erosion at the last glacial maximum revealed by thermoluminescence thermochronometry, Quat. Geochronol.,73, 101405, https://doi.org/10.1016/j.quageo.2022.101405, 2022.

Tarantola, A.: Inverse problem theory and methods for model parameter estimation, SIAM, 342 pp., https://doi.org/10.1137/1.9780898717921, 2005.

Toyoda, S., and Ikeya, M.: Thermal stabilities of paramagnetic defect and impurity centers in quartz: Basis for ESR dating of thermal history, Geochem. J., 25(6), 437-445, https://doi.org/10.2343/geochemj.25.437, 1991.

Tsukamoto, S., Toyoda, S., Tani, A., and Oppermann, F.: Single aliquot regenerative dose method for ESR dating using X-ray irradiation and preheat, Radiat. Meas., 81, 9-15, https://doi.org/10.1016/j.radmeas.2015.01.018, 2015.

Valla, P.G., Lowick, S.E., Herman, F., Champagnac, J.D., Steer, P., and Guralnik, B.: Exploring IRSL50 fading variability in bedrock feldspars and implications for OSL thermochronometry, Quat. Geochronol., 36, 55-66, https://doi.org/10.1016/j.quageo.2016.08.004, 2016.

Visocekas, R., Spooner, N.A., Zink, A., and Blanc, P.: Tunnel afterglow, fading and infrared emission in thermoluminescence of feldspars, Radiat. Meas., 23(2-3), 377-385, https://doi.org/10.1016/1350-4487(94)90067-1, 1994.

Wen, X., Bartz, M., and King, G.K.: ESR and luminescence thermochronometry of the Rhône valley, Switzerland, Quaternary GChron., 80, 101496, https://doi.org/10.1016/j.quageo.2023.101496, 2024.

Wheelock, B., Constable, S., and Key, K.: The advantages of logarithmically scaled data for electromagnetic inversion, Geophys. J. Int., 201(3), 1765-1780, https://doi.org/10.1093/gji/ggv107, 2015.

Wintle, A.G.: Anomalous fading of thermo-luminescence in mineral samples, Nat., 245(5421), 143-144, https://doi.org/10.1038/245143a0, 1973.

Wu, T.S., Jain, M., Guralnik, B., Murray, A.S., and Chen, Y.G.: Luminescence characteristics of quartz from Hsuehshan Range (Central Taiwan) and implications for thermochronometry, Radiat. Meas., 81, 104-109, https://doi.org/10.1016/j.radmeas.2015.03.002, 2015.

Zhang, J., Arriga, G., Rossetti, F., Argante, V., Kraemer, D., Sontag-González, M., Cosentino, D., Cipollari, P., and Tsukamoto, S.: Dolomite luminescence thermochronometry reconstructs the low-temperature exhumation history of carbonate rocks in the central Apennines, Italy, Comm. Earth Environ, 6, 252, https://doi.org/10.1038/s43247-025-02216-1, 2025.